Available online at www.sciencedirect.com
ScienceDirect
Polymer 48 (2007) 3565–3573
polymer
www.elsevier.com/locate/polymer

Microphase separation in amorphous poly(imide siloxane) segmented copolymers

Chun-Kang Ku, Yu-Der Lee*

Department of Chemical Engineering, National Tsing Hua University, Hsinchu 30013, Taiwan, ROC

Received 2 November 2006; received in revised form 23 March 2007; accepted 15 April 2007
Available online 21 April 2007

Abstract

A series of amorphous poly(imide siloxane) (PIS) segmented copolymers with various segmental lengths and contents of poly(dimethyl siloxane) (PDMS) were synthesized by condensation polymerization. Extraction was utilized to obtain highly pure PISs for a study of phase separation. The PISs self-assemble from dilute solutions that are initially rod-like structures and then rapidly transform to vesicles. Moreover, the vesicles change to solid spheres as the PDMS content increases. A variety of morphologies of the PIS films, including unilamellar vesicle, multilamellar vesicle, sea-island and others, are found as a function of the content and the segmental length of PDMS. Small angle X-ray scattering demonstrates the coexistence of large-scale phase separations and nano-scale phase separations of approximately 20 nm. The DSC results reveal that the phase separation is induced and dominated by the aggregation of PDMS segments. Furthermore, the surfaces of the hard phases in the PDMS-900 PISs are found to be fractal.

Keywords: Polyimide; Poly(imide siloxane); Microphase separation

1. Introduction

Excellent adhesive properties, good gas permeability, low dielectric constants, ease of processability, and favorable overall thermal and mechanical properties have led to poly(imide siloxane) (PIS) copolymers' becoming an important branch of novel polyimides, extensively studied in applications of photosensitive films, gas-permeable membranes and adhesives, etc [1–5]. However, PIS copolymers are much more complicated than the polyimide homopolymers in that two components are involved, which have a low mixing entropy. This low mixing entropy results in the microphase separation of PIS, with a domain size that varies with the block length and the content of PDMS. Accordingly, a co-solvent system, in which one solvent favors the poly(dimethyl siloxane) (PDMS) component and the other prefers the polyimide component, must be adopted for the synthesis. The morphology and the extent of aggregation vary with numerous variables, such as composition, block length, processing conditions (including annealing and casting solvent) and block sequence distribution. Additionally, the minimization of the surface free energy leads to an enrichment of the surface with a component that has siloxane with a low surface free energy [6–11].

Even though several investigations have noted that the PIS exhibits phase separation, related studies are few. Tiwari and Nema blended the precursor of polyimide with PDMS and found that, after the solvent was extracted, the PDMS was present as dispersed spheres at microlevel in the polyimide medium [12]. Arnold et al. synthesized a series of polyimide–PDMS segmented copolymers and two glass transition temperatures (T_gs) were found, demonstrating that the segments were well separated. Moreover, the higher T_g was a function of both the content of incorporated siloxane and the molecular weight of siloxane. It increased with the molecular weight of siloxane and as the amount of incorporated siloxane declined [13]. Applying the dynamic mechanical

* Corresponding author. Tel.: +886 3 5713204; fax: +886 3 5715408.
E-mail address: ydlee@che.nthu.edu.tw (Y.-D. Lee).

0032-3861/$ - see front matter © 2007 Elsevier Ltd. All rights reserved.
doi:10.1016/j.polymer.2007.04.028

analysis, Furukawa et al. proved that the PIS copolymer had two glass transition temperatures – a direct evidence of the phase separation. The large decrease in the higher T_g as the PDMS content increased indicated a partially miscible state between the two segments at high temperature. The long PDMS segments are preferentially segregated from the polyimide phase, forming large domains and, therefore, a sea-island structure formed [14].

Unlike in controlled polymerization, such as ionic polymerization or living radical polymerization, polymers obtained by polyaddition or polycondensation exhibit only short-range microphase separation because of their broad polydispersity distribution [15], causing a problem in studying the phase separation of PIS copolymers in detail. This is the primary reason for the lack of literature on the phase separation of PIS. Unlike in the literature, one of the most important features of this study is that highly pure PIS segmented copolymers, with narrower polydispersity distributions than the controlled ones, are obtained via extraction. By employing these purified copolymers, the morphological nature and the phase separation of the PIS segmented copolymers are disclosed and discussed in more detail than they have been before.

2. Experimental

2.1. Materials

4,4′-Oxydiphthalic dianhydride (ODPA) and 1,3-bis(4-aminophenoxy) benzene (APB) were purchased from Chriskev (Leawood, Kansas, USA) and Mitsui Chemicals (Tokyo, Japan), respectively. α,ω′-Aminopropylpoly(dimethyl siloxane) (PDMS) with various segmental lengths ($M_n = 900$, 1680, and 4600) was purchased from Shinetsu Chemicals (Tokyo, Japan). ODPA was recrystallized from acetic anhydride. APB was recrystallized from methanol. PDMS was dehydrated with a molecular sieve (type 4A, Aldrich). *N*,*N*-Dimethyl acetamide (DMAc) and tetrahydrofuran (THF) were both purchased from Tedia (Fairfield, Ohio, USA) and the former was dehydrated by mixing it with calcium hydride for 12 h in nitrogen, followed by vacuum distillation. THF was dehydrated by mixing it with sodium metal under nitrogen until the indicator, benzophenone, turned dark blue and then THF was distilled. According to Carl–Fischer titration, the water content of the purified monomers and the solvents was less than 100 ppm. The dehydrated PDMS, DMAc and THF were stored in hermetical vials, which were filled with dry nitrogen, before use.

2.2. Synthesis of poly(imide siloxane) precursor

Scheme 1 outlines the synthetic route to the poly(imide siloxane) segmented copolymers. All polymerizations were carried out in flowing nitrogen, and equimolar amounts of diamine and dianhydride monomers were used in all cases. The hard segments are based on ODPA and APB. The soft segment is PDMS. Since PDMS does not dissolve in DMAc, a co-solvent system is essential. DMAc and THF were used as the co-solvent in a weight ratio of 1:1. The polymerization procedure was as follows. The THF solution of appropriate amount of PDMS was added dropwise to a magnetically stirred DMAc solution of excess ODPA under dry nitrogen. The reaction proceeded at room temperature for 12 h and then a suitable amount of APB was added. The reaction was continued for another 12 h to yield the precursor, poly(amic acid), a solution with a solid content of 20 wt.%.

2.3. Purification of poly(imide siloxane) precursor

Although the monomers and the solvents were purified before use, and the polymerization conditions were strictly controlled, the presence of unreacted monomers, uncoupling ODPA–PDMS and ODPA–APB homopolymers could not be prevented. The crude precursors were firstly precipitated and washed with methanol/water in a volume ratio of 2:1 to remove the unreacted monomers and the uncoupled ODPA–PDMS precursors, while they dissolved in the mixed solvent but the PIS and the uncoupled ODPA–APB precursors did not. Then, the desirable PIS precursors were extracted using acetone/water in a volume ratio of 5:1, leaving the uncoupled ODPA–APB precursors. After the acetone in the extract was evaporated, the PIS precursors, which precipitated from water, were filtered and dried at 70 °C in vacuo for 12 h.

2.4. Formation of poly(imide siloxane) copolymers films

The DMAc/THF, in a weight ratio of 1:1, solution of the purified PIS precursor with a solid content of 15 wt.% was cast on a Teflon mold, before being cyclodehydrated according to the heating protocol, as follows: room temperature to 70 °C at a heating rate of 1.5 °C/min, equilibrium at 70 °C for 30 min, heat to 170 °C at a rate of 1.5 °C/min, equilibrium at 170 °C for 1 h, heat to 250 °C at a rate of 2 °C/min, and equilibrium at 250 °C for 2 h. The PIS films with a thickness of 60–80 μm were obtained.

2.5. Measurements

2.5.1. ^1H nuclear magnetic resonance (^1H NMR)

A trimethyl silane free deuterated dimethyl sulfoxide (DMSO-d_6) was applied as a solvent. The ^1H NMR spectra of the PIS precursors were recorded on a Varian Uniytinova-500 spectrometer.

2.5.2. Gel permeation chromatography (GPC)

The apparent molecular weight distributions of PIS precursors were measured at 25 °C using a GPC system, which consisted of a Waters 510 HPLC pump, a Phenomenex Phenogel column (10^4 Å), and a Waters 410 differential refractive index detector, with 0.05 wt.% $LiNO_3$-containing dimethyl acetamide (DMAc) at a flow rate of 0.7 mL/min. Linear polystyrene was employed as a calibration standard, with ChromManager software from the Analytical Based Development Center (ABDC, Taiwan). A Phenomenex Phenogel linear column was used as an alternative and the eluent was DMAc without any additives to understand the extraction.

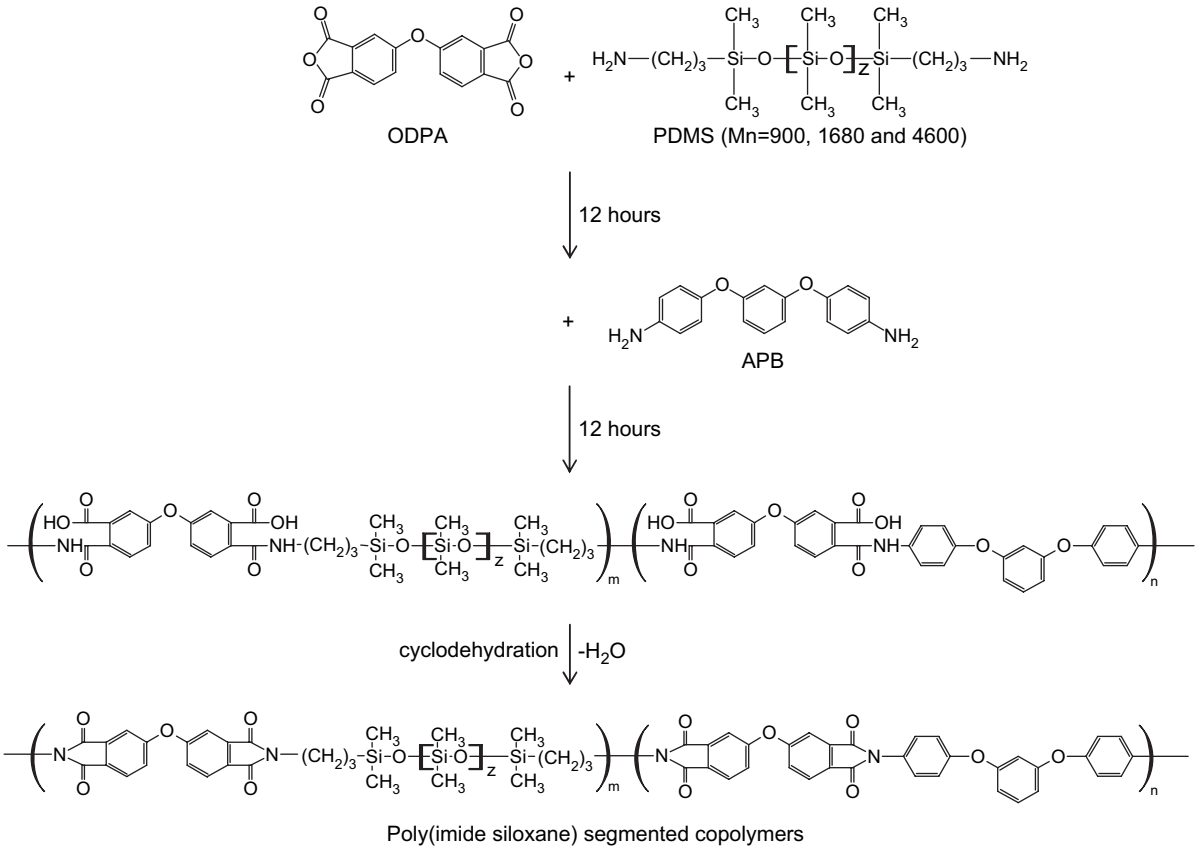

Scheme 1. Synthetic route of poly(imide siloxane) segmented copolymers.

2.5.3. Transmission electron microscopy (TEM)

TEM was performed on a JOEL JEM-1230 microscope, with a Gatan DualVision CCD Camera, at an acceleration voltage of 80 kV. The precursors were dissolved in DMAc/THF, in a weight ratio of 1:1, to form a dilute solution at a concentration of 0.2 wt.%. A drop of the dilute solution was then deposited on an EM copper grid, which had been precoated with carbon. The excess solvent was carefully blotted away using a strip of filter paper. The samples were dried by stepwise heating to 250 °C, the cyclodehydrating temperature, and then being held at equilibrium for 2 h. Finally, the samples were cooled to room temperature at a rate of −20 °C/min.

2.5.4. Optical microscopy (OM)

The morphology of the PIS films was observed using an Olympus BH2-UWA optical microscope, with a TOSHIBA IK-637F CCD, in reflection mode.

2.5.5. Small angle X-ray scattering (SAXS)

The SAXS experiment was conducted on a Bruker Nanostar SAXS instrument. The X-ray source, a 1.5 kW X-ray generator (Kristalloflex 760) equipped with a Cu tube, was operated at 35 mA and 40 kV. The scattering intensity was measured by a two-dimensional position-sensitive detector (Bruker AXS) with 512×512 channels. The area scattering pattern was radially averaged to increase the photon counting efficiency compared with the one-dimensional linear detector. The intensity profile was output as a plot of the scattering intensity (I) vs. the scattering vector, $q = 4\pi/\lambda \sin(\theta/2)$ (θ = scattering angle). All scattering data were corrected by the empty beam scattering, the sensitivity of each pixel of the area detector and the thermal diffuse scattering (I_{TDS}).

2.5.6. Wide angle X-ray scattering (WAXS)

WAXS works were performed using a SCINTAG ID 3000 diffractometer. Ni-filtered X-ray radiation from a copper tube (accelerating voltage was 40 kV, electric current was 35 mA) was used. A position-sensitive detector (ThermoARL) was utilized and the scattering angle was calibrated by quartz. The sample-to-detector distance was 16 cm. Diffraction data were collected over an angular range of $2^\circ < 2\theta < 90^\circ$ in steps of 0.02°, with 1 min at each 4°.

2.5.7. Differential scanning calorimetry (DSC)

DSC experiments were performed using a Perkin–Elmer Diamond DSC equipped with a liquid nitrogen cooler in a helium atmosphere. The temperature and the heat capacity were calibrated with indium and mercury. The sample weight was in a range of 15–20 mg. The sample was cooled to −150 °C at a rate of −20 °C/min and then scanned up to 300 °C at a rate of 20 °C/min. This procedure was repeated and the second run was recorded.

3. Results and discussion

3.1. Synthesis of highly pure poly(imide siloxane) precursor, poly(amic acid)

The composition of PISs was calculated from the ^{1}H NMR spectra of their corresponding precursors. By comparing the peak area of the methyl hydrogen appended to the silicon of the PDMS ($\delta = 0$ ppm) with that of the *ortho*-phenyl hydrogen of the APB ($\delta = 6.72-6.82$ ppm), the number of PDMS segments with respect to one APB segment could be calculated, such that the weight fraction of soft segment (WFSG) was obtained.

Table 1 presents the composition and the GPC results. The sample code is expressed as *xxx-yy*, where *xxx* denotes the number-average molecular weight of the PDMS segment, and *yy* is the weight percentage of the soft (PDMS) segment in the copolymers. Since the PIS precursor, poly(amic acid), in DMAc exhibits weak polyelectrolyte characteristics, the ''Coulomb repulsion'' causes the linear polyelectrolyte chain to adopt a more expanded, rigid-rod-like conformation. Consequently, when the molecular weight of PIS precursor is measured by size exclusion chromatography (SEC), some salt must be added to the eluent to screen the charges in the polyelectrolytes to avoid overmeasurements of molecular weight [16,17].

The precursors of the PIS and the ODPA–APB are more easily separated by SEC in expanded state because of the size difference between the precursors of PIS and ODPA–APB in expanded state is larger than that in collapsed state. Therefore, the GPC experiment was performed using a pure DMAc as eluent to examine the efficiency of extraction. However, this experiment risks blocking and damaging the column because of the large size of the expanded precursors.

Fig. 1 displays the GPC traces of the 900-27 before and after extraction. The precipitated 900-27 clearly has two maxima at $t = 11.05$ min and $t = 19.74$ min, respectively, evidencing the presence of ODPA–APB and PIS precursors. Following the extraction, the former peak completely disappears, suggesting that the ODPA–APB precursor is totally removed from the precipitate. Furthermore, the latter peak is sharper and shifts to a longer elution time revealing that the partial PIS precursor with higher molecular weight is also moved out. However, the decrease in polydispersity facilitates the phase separation of PIS.

Table 1
Composition and GPC results of PISs

Sample code	WFSG in feed (wt.%)	Calculated WFSG (wt.%)	M_n	M_w/M_n
900-27	10	27	6125	1.20
900-35	25	35	6478	1.22
900-41	50	41	9990	1.41
900-64	75	64	6935	1.28
1680-43	50	43	8561	1.34
4600-46	50	46	7867	1.34

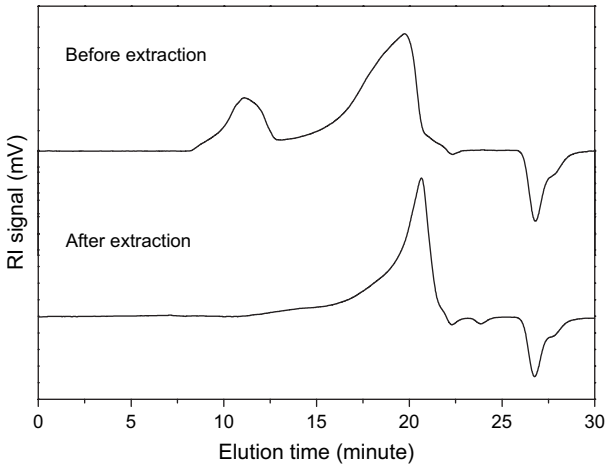

Fig. 1. GPC trace of 900-27 before and after extraction.

3.2. Gel permeation chromatography (GPC)

Unlike anionic or other controlled polymerization, condensation polymerization does not easily yield copolymers with narrow polydispersity and does not allow the molecular weight to be controlled precisely. As shown in Table 1, the polydispersity and the molecular weight of PIS precursors increase with the PDMS content to a WFSG of 41 wt.% and fall as WFSG reaches 64 wt.%. The reactivity of APB is better than that of PDMS; however, some ODPA is hydrolyzed in the first-stage reaction, reducing the quantity of APB that couples to the PIS mainchain in the second-stage reaction. The competition between these two factors leads to a compromise whereby the PIS precursor has the highest molecular weight and the largest polydispersity at which the amounts of PDMS and APB are almost identical. Moreover, the drop in the molecular weight as the segmental length of PDMS increases is ascribed to the decline in the concentration of $-NH_2$ and the increase in the viscosity.

3.3. Morphology from a dilute solution

Before investigating the phase separation of the PIS films from concentrated solutions, the morphological nature of the PISs from dilute solutions must be understood. Table 2 presents the solubility parameters (also called Hildebrand parameters) of the segments and the solvents. The solubility parameter of ODPA–APB segment is calculated using the molar group contribution approach [18,19]. Apparently, the DMAc is

Table 2
Solubility parameters (δ) of pure segments and solvents

Segment	δ $(J/m^3)^{1/2} \times 10^{-3}$	Solvent	δ $(J/m^3)^{1/2} \times 10^{-3}$
PDMS	15.1[a]	THF	18.6[c]
ODPA–APB	22.5[b]	DMAc	22.1[c]

[a] Ref. [28].
[b] Calculated by molar group contribution approach.
[c] Ref. [18].

a good solvent for the ODPA–APB segment, but a poor solvent for the PDMS segment. However, the boiling temperature of DMAc ($T_b = 165$ °C) is much higher than that of THF ($T_b = 66$ °C). Once the THF is removed upon heating, the difference in solubility parameter between PDMS and DMAc causes the association of PDMS segments. Accordingly, the inconsistency of solubility parameter between the PDMS segment and the high-boiling-point aprotic solvent is the main reason for the phase separation, even though many studies have mentioned that the phase separation is predominated by the low mixing entropy between the PDMS segment and the polyimide segment [6–11,13,14]. The TEM images, shown in Fig. 2, reveal that the morphologies of the PISs from dilute solutions change from vesicles to solid spheres as the PDMS content increases. In 900-27, most of the aggregates are closed vesicles; nevertheless, some open vesicles remain, as indicated by the arrows. The intermediate structures manifest that the PISs initially aggregate as rod-like structures and then transform to vesicles rapidly via the bending of rods (as indicated by arrow 1), resulting from the asymmetrical interaction, or the head-to-head combinations of rods (indicated by arrow 2). The concentration effect is such that as the PDMS content increases, the aggregates become solid spheres. Comparing the 900-41 with the 4600-46 clearly reveals that the association among the aggregates increases with the PDMS segmental length, making them more irregularly shaped. Moreover, the fact that partial amount of PDMS segments mix with PI segments (see Section 3.6) and the difficulty to obtain a well-defined copolymer structure by polycondensation make the discrepancy between the actual amount of PDMS and the amount of PDMS aggregates observed in TEM.

3.4. Surface morphology of PIS films

The surface topography of PIS films was observed under OM, as displayed in Fig. 3. Their morphologies are very similar to those of films prepared from dilute solutions. The surface morphology varies as a strong function of the content and the segmental length of PDMS. In the 900-27, many unilamellar vesicles are observed. The irregular multilamillar vesicles are present in the 900-41, and a sea-island structure is observed as the PDMS content increases further to 64 wt.%. Since the surface free energy of PDMS is lower than that of ODPA–APB PI segment, the PDMS segments tend to aggregate and segregate to the surface to minimize the total free energy of the system [6–11], causing a difference in surface energy between the PDMS-rich phase and the PDMS-poor phase to induce an uneven surface topography. As the PDMS segmental length increases, the morphology tends to be bicontinuous.

As well as micro-scale domains, many small aggregates, which are invisible under OM, are present, the fact being supported by small angle X-ray scattering.

3.5. Small angle X-ray scattering (SAXS)

The PIS films were probed using SAXS to verify the nanoscale aggregates. The domain size d can be estimated from the q_m, corresponding to the maximum of the $I(q)$ vs. q profiles, according to the Bragg's equation [20,21]:

$$d = 2\pi/q_m \tag{1}$$

In Fig. 4, the unusually strong intensity at $q = 0.1$ nm^{-1} results from the large-scale inhomogeneity. The domain size d in

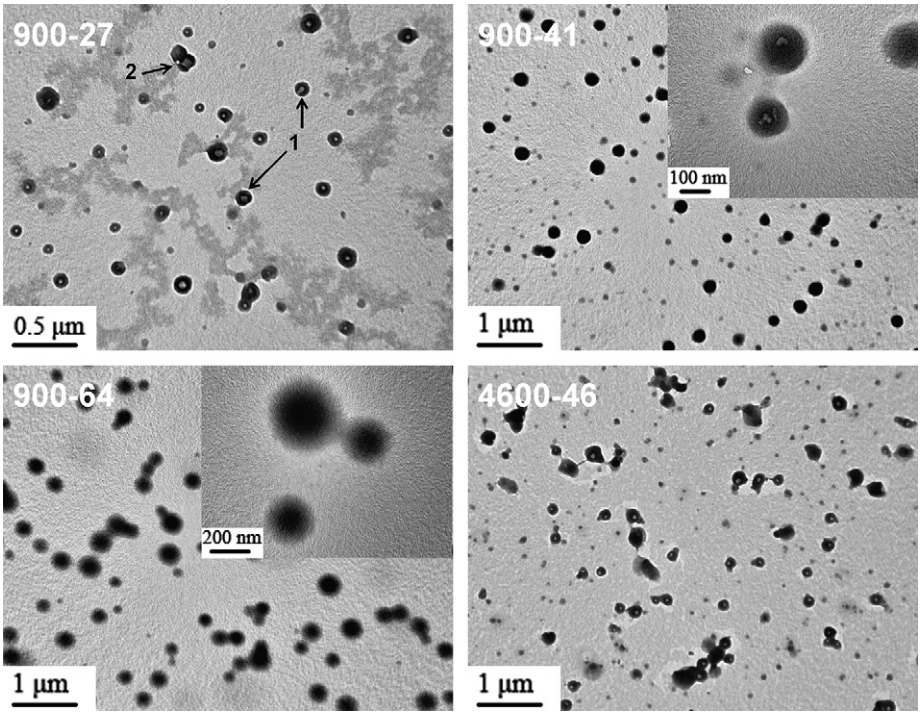

Fig. 2. TEM images of PISs. Observations were performed directly without staining. The dark region appears to be the PDMS aggregate.

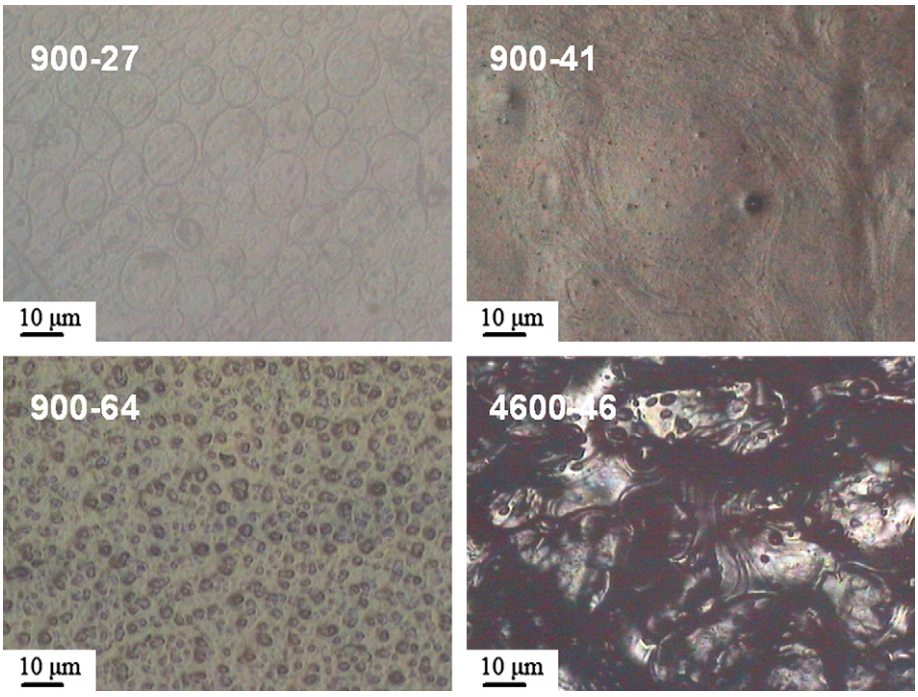

Fig. 3. Surface morphologies of PISs.

the proximity of 20 nm, irrespective of the subsidiary peak at $q = 0.313\ \mathrm{nm}^{-1}$, is evidence of the presence of nano-scale aggregates in the PIS films. The scattering peak height is roughly proportional to the contrast between the phases. Hence, the peak intensity at $q = 0.313\ \mathrm{nm}^{-1}$ depends on the PDMS content and is greatest on 900-41, associated with the maximal nano-scale phase separation. In Fig. 5, as the segmental length of PDMS increases, the intensity and the position of the subsidiary peak do not change, but the increase in the peak intensity at $q = 0.1\ \mathrm{nm}^{-1}$ indicates that the degree of large-scale separation ($d > 63$ nm) increases with the length of the PDMS segment. In summary, in the PDMS-poor region, the degree of large-scale phase separation diminishes gradually as the PDMS is added. Furthermore, the degree of nano-scale separation is greatest at a PDMS content of 41 wt.%. The PDMS segmental length does not influence the size and the degree of the nano-scale separation, but the degree of the large-scale separation slightly increases with the segmental length of PDMS suggesting that the association among the small aggregates increases as well.

3.6. Differential scanning calorimetry (DSC)

Wide angle X-ray scattering yields an amorphous halo at 21° without any other peaks, indicating that they are all amorphous which is corroborated by the DSC results.

Fig. 6 is the DSC plots of the PIS films. The Fox equation [22], the most generally accepted form of empirical origin for

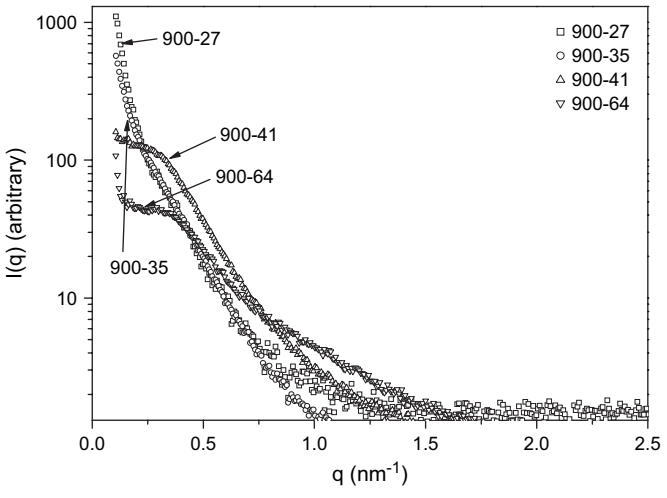

Fig. 4. SAXS intensity profiles of PDMS-900 PISs.

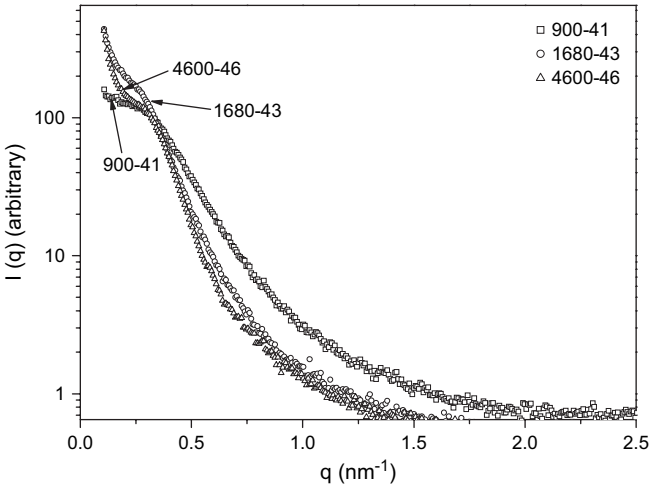

Fig. 5. SAXS intensity profiles of PISs with different segmental lengths of PDMS.

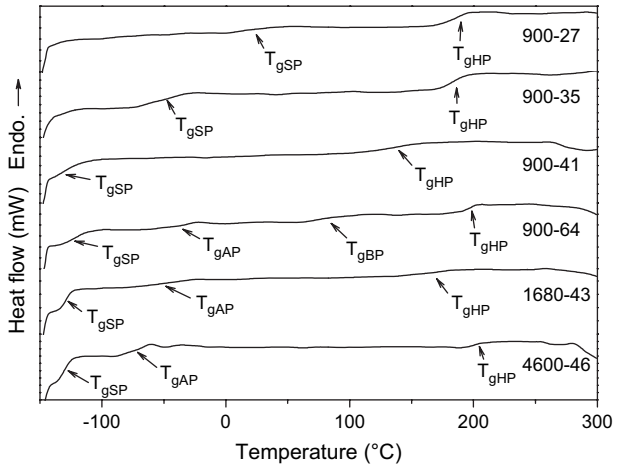

Fig. 6. DSC thermograms of PISs.

characterizing the change in thermal properties of a single phase two-component system, and the mass balance equation are applied to calculate the composition of the phases in the PIS films.

Fox equation:

$$1/T_g = W_S/T_{gS} + W_H/T_{gH} \quad (2)$$

Mass balance of the soft segment:

$$W_S = W_{SP}W_{SS} + W_{HP}W_{SH} \quad (3)$$

Table 3 summarizes all the calculated results. Table 4 is a glossary of terms. For the PDMS-900 PISs, the difference between the T_gs of the two phases increases as the PDMS content increases from 27 wt.% to 41 wt.%, indicating that the phase separation increases severely. If the PIS films are assumed to be homogeneous, the Fox equation can be used to calculate the T_g of each PIS film, T_{gm}. As the PDMS content increases, the $|T_{gm} - T_{gHP}|$ remains almost constant in the range 160–180 °C, but the $|T_{gm} - T_{gSP}|$ increases markedly. This fact demonstrates that the extent of phase separation in this system is mainly predominated by the soft phase. Based on the fact that the soft phase approaches pure PDMS as the PDMS content increases, the phase separation is driven and dominated by the PDMS because of its remarkably high mobility and the thermodynamic incompatibility between the PDMS segment and its environment. From another perspective, the increase in PDMS content is equivalent to the decline in hard segment content, and the hard-chain length [23]. The PDMS segments are bound by the hard segments, causing the mobility of PDMS segment to depend more or less on the hard-chain length. The hard segment is less mobile than the PDMS and, consequently, the trammels of the PDMS increases with the hard-chain length. Moreover, when the PDMS content is low, the inter-PDMS distance between two neighboring polymers is too far for PDMS to aggregate. These two contributions cause the PDMS segments to mix well with the hard segments at low PDMS content. The 900-27 can almost be regarded as homogeneous. As the PDMS content increases, the trammel falls and the concentration of PDMS segments increases, improving the aggregation of PDMS segments, such that the phase separation becomes more significant. Until the PDMS content reaches 41 wt.%, the soft phase comprises only pure PDMS ($T_g = -123$ °C), the fact which is a powerful evidence of the aggregation of PDMS segments. The largest $|T_{gHP} - T_{gSP}|$ and the purest soft-phase composition suggest that the 900-41 exhibits the most phase separation. With reference to the literature, the densities of the soft segment (ρ_S) and the hard segment (ρ_H) are 1.000 and 1.246 g/cm^3, respectively [19]. Thus, the volume fraction of soft segment in the 900-41 is found to be 47 vol.%, which result is consistent to the general phenomenon of polymer blends that the most phase separation occurs at which the volume fraction of either component is 50 vol.% [24]. As the PDMS content increases to 64 wt.%, four separated phases

Table 3
DSC results of PISs

Sample code	T_g (°C)	Phase	Breadth (°C)	Weight fraction of soft segment	Weight fraction of hard segment	Weight fraction of phase	$\lvert T_{gm} - T_g \rvert$ (°C)
PDMS	−123	–	–	–	–	–	–
ODPA–APB	221	–	27	–	–	–	–
900-27	29	Soft	29	0.277	0.723	0.959	4
	195	Hard	24	0.024	0.976	0.041	162
900-35	−56	Soft	48	0.557	0.443	0.603	57
	181	Hard	57	0.038	0.962	0.397	180
900-41	−125	Soft	20	1	0	0.368	106
	155	Hard	62	0.067	0.933	0.632	174
900-64	−134	Soft	5	1	0	NA	61
	−33	A	29	0.461	0.539	NA	40
	78	B	41	0.178	0.822	NA	151
	184	Hard	20	0	1	NA	257
1680-43	−129	Soft	18	1	0	NA	99
	−27	A	50	0.44	0.56	NA	3
	185	Hard	46	0.034	0.966	NA	209
4600-46	−130	Soft	18	1	0	NA	90
	−74	A	48	0.646	0.354	NA	41
	200	Hard	15	0	1	NA	233

NA: not available.

Table 4
Glossary of DSC terms

T_{gm}	Glass transition temperature of PIS in homogeneous state
T_{gH}	Glass transition temperature of pure hard segment
T_{gS}	Glass transition temperature of pure soft segment
T_{gHP}	Glass transition temperature of hard phase
T_{gSP}	Glass transition temperature of soft phase
T_{gAP}	Glass transition temperature of phase A
T_{gBP}	Glass transition temperature of phase B
W_H	Weight fraction of hard segment in the copolymer
W_S	Weight fraction of soft segment in the copolymer
W_{HP}	Weight fraction of hard phase
W_{SP}	Weight fraction of soft phase
W_{HS}	Weight fraction of hard segment in the soft phase
W_{SS}	Weight fraction of soft segment in the soft phase
W_{HH}	Weight fraction of hard segment in the hard phase
W_{SH}	Weight fraction of soft segment in the hard phase

form, making it unable to calculate the phase content. For the PDMS-rich PIS films, the large incompatibility between the PDMS segments and the hard segments increases the complexity of phases.

It is worth to notice that the T_{gSP} of 900-41 is slightly lower than the reported T_g of PDMS (T_{gS}). For a polymer at a temperature below its T_g, only local motion of individual chain is present, without cooperation between chains. Nevertheless, at the onset of the T_g, the cooperation involves numerous molecules and increases as the temperature approaches T_g. Therefore, the confinement of molecular motion affects the dynamic properties, such as dielectric relaxation and T_g, when the confining dimensions are comparable to the cooperative scale [25,26]. Haralampus et al. asserted that the nano-scale confinement reduces the cooperative length and increases the rotational mobility near T_g and T_g is depressed [25]. We believe that the surprising low T_{gSP} shown in the 900-41 is caused by nano-confinement effect. The nano-confinement effect is also observed on 1680-43 and 4600-46. Additionally, some investigations have reported that PDMS exhibits a cold crystallization at −85 °C and two melting endothermic peaks at −46 and −40 °C [27,28]. However, in this study, nano-confinement prevents the crystallization of PDMS segment, even the long-range order of PDMS segment is still difficult to be obtained. The hard phases of the 900-64 and the 4600-46 are believed to be the agglomeration of hard segments because of their narrow breadths of T_{gHP}; however, the decline in T_{gHP}, which is compared to the T_{gH} (T_g of ODPA−APB homopolymer), is attributed to the reduction in molecular chain length.

Undoubtedly, the compositions and the contents of the soft phases and the hard phases vary with the PDMS content. For the PDMS-900 PIS films, as the PDMS content increases from 27 wt.% to 41 wt.%, the PDMS content does not influence the composition of hard phase as much as it does for the soft phase. For a well separated system, the hard phase content should increase with the hard segment content; however, this phenomenon is not observed herein. As the THF is removed upon cyclodehydration, the aggregation of PDMS is induced by the difference in solubility parameter between PDMS and DMAc. Such aggregation of PDMS and the thermodynamic incompatibility between PDMS and hard segment exclude the hard segments from the soft phases to form the hard phases. As a consequence, the aggregation of PDMS increases with its content, also increasing the hard phase content.

The number of the soft segment in the hard phase (N_{SH}) and the characteristic length of the hard phase (l_H) can be calculated according to the following equations.

$$N_{SH} = W_{HP} \times W_{SH}/(\text{molecular weight of PDMS}) \quad (4)$$

$$l_H = [W_{HP}/(\rho_S \times W_{SH} + \rho_H \times W_{HH})]^{1/3} \quad (5)$$

The calculated results are listed in Table 5. The N_{SH} and l_H can be correlated to obtain the scaling law:

$$N_{SH} = 9.27 \times 10^{-5} l_H^{3.95} \quad (6)$$

According to the thermodynamic incompatibility between the soft segment and the hard segment and the extremely low soft segment content in the hard phase, it is plausible that the soft segments disperse on the surface of the hard phase, resulting from the insufficient mobility of the soft segments close to the junctions between soft segments and hard segments. From this origin, the number of the soft segment on the surface of hard phase (N_{SH}) is proportional to the characteristic length of hard phase (l_H) to a power of 3.95 which suggests the fractal surface of the hard phase, whereas N_{SH} is proportional to l_H squared represents a regular and smooth surface.

The mixing of two different components results in an increase in the breadth of T_g. However, as the PDMS content increases, despite the fact that the mixing extent of the hard phase is much less than that of the soft phase, the breadth of T_{gHP} increases more rigorously than that of T_{gSP}. Consequently, we speculate that the breadth of T_g is a function of not only the mixing extent but also of the dispersive condition. The PDMS segments are reasonably considered to disperse well in the soft phase because of its high content; however, the PDMS segments reside only on the surface of the hard phase. The dispersion of PDMS segments in the hard phase is not as homogeneous as that in the soft phase and therefore the hard phase is more inhomogeneous, exhibiting both compositional inhomogeneity and dispersive inhomogeneity, broadening the breadth. This fact strengthens the claim that the PDMS segments are dispersed on the surface of the hard phase.

Unlike PDMS-900 PIS films, PDMS-1680 and PDMS-4600 PISs show three separate phases, however, the content of each phase cannot be calculated as described above. Despite this fact, the composition of the phase can be still determined

Table 5
Number of soft segment in hard phase (N_{SH}) and characteristic length of hard phase (l_H)

Sample code	$N_{SH} \times 10^{-5}$	l_H
900-27	0.109	0.321
900-35	1.676	0.685
900-41	4.705	0.801

Calculations are based on unit weight of sample.

using the Fox equation. The increase in segmental length typically enhances the inhomogeneity between segments, intensifying the phase separation. As the mobility of PDMS increases with its segmental length, the aggregations of PDMS segments become significant and the resulting exclusion effect improves the conglomeration of hard segments. The $|T_{gm} - T_{gAP}|$ and the $|T_{gm} - T_{gSP}|$ increase with the segmental length of PDMS, as is evidence of the increase in the degree of phase separation, driven by the PDMS segments.

4. Conclusions

A series of amorphous poly(imide siloxane)s with different PDMS contents and segmental lengths were synthesized via condensation polymerization and then purified to study the phase separation phenomenon. Choosing a suitable solvent enables the highly pure PIS precursors to be obtained via extraction. From a dilute solution, the PISs aggregate from vesicles to solid spheres as the PDMS content increases. For the PDMS-900 PIS films, the unilamellar and multilamellar vesicles are present when the PDMS content is less than 41 wt.%, transforming to sea-island structures as the PDMS content increases to 64 wt.%. Furthermore, the morphology tends toward bicontinuous as the segmental length of PDMS increases. The SAXS results further prove that the micro-scale domains result from the agglomeration of numerous nano-scale aggregates with a domain size of about 20 nm. This agglomeration increases with the segmental length of PDMS. Among the PDMS-900 PIS films, the nano-scale phase separation is the greatest at a PDMS content of 41 wt.%, which corresponds to the DSC results. The DSC result reveals that the phase separation of PIS is driven and dominated by PDMS. The phase separation of PIS is initially induced by the aggregation of PDMS segments due to the difference in solubility between the PDMS and the aprotic solvent. During the aggregation of PDMS segments, the hard polyimide segments are excluded simultaneously from soft phases by the thermodynamic incompatibility between PDMS segment and polyimide segment. In the PIS film with a low PDMS-900 content, the trammels on the mobility of PDMS and the low concentration of PDMS cause the PDMS segments to mix well with the hard segments. The aggregation of PDMS segments increases with PDMS content. Accordingly, the phase separation increases with PDMS content and is most significant on a PDMS-900 content of 41 wt.%, which is equivalent to 47 vol.%. Partial phase mixing makes the phases more complex as the PDMS content increases further to 64 wt.%. For PDMS-900 PISs, the scaling law, $N_{SH} = 9.27 \times 10^{-5} l_H^{3.95}$, indicates that the surface of the hard phase is fractal. Additionally, the nano-confinement effect causes the T_g of PDMS aggregate to be slightly lower than that of bulk PDMS. The incompatibility between PDMS segment and hard segment increases with the segmental length of PDMS. Consequently, a PIS with longer PDMS segment exhibits more intense phase separation.

Acknowledgements

The authors would like to thank the National Science Council of the Republic of China, Taiwan, for financially supporting this research under Contract No. NSC 95-2622-E-007-001. Prof. Shin-Lung Chen of the Department of Chemical Engineering, National Tsing Hua University, Taiwan, is appreciated for valuable discussion regarding the SAXS data.

References

[1] Kang JH, Cho K, Park CE. Polymer 2001;42:2513–20.
[2] Nakagawa T, Nishimura T, Higuchi A. J Membr Sci 2002;206:149–63.
[3] Chen SH, Lee MH, Lai JY. Eur Polym J 1996;32:1403–8.
[4] Kang JH, Cho K, Park CE. J Adhes Sci Technol 2001;15:913–28.
[5] Jin XZ, Ishii H. J Photopolym Sci Technol 2004;17:201–6.
[6] Andre S, Pietrasanta FG, Rousseau A, Boutevin B. J Polym Sci Part A Polym Chem 2001;39:2414–25.
[7] Ha SY, Oh BK, Lee YM. Polymer 1995;36:3549–53.
[8] Zhao J, Rojstaczer SR, Gardellar Jr JA. J Vac Sci Technol A 1998;16: 3046–51.
[9] Zhao J, Rojstaczer SR, Chen J, Xu M, Gardellar Jr JA. Macromolecules 1999;32:455–61.
[10] Mahoney CM, Gardella Jr JA, Rosenfeld JC. Macromolecules 2002;35: 5256–66.
[11] Park HB, Han DW, Lee YM. Chem Mater 2003;15:2346–53.
[12] Tiwari A, Nema SK. Mater Res Innov 2003;7:133–43.
[13] Arnold CA, Summers JD, Chen YP, Bott RH, Chen D, McGrath JE. Polymer 1989;30:986–95.
[14] Furukawa N, Yamada Y, Furukawa M, Yuasa M, Kimura Y. J Polym Sci Part A Polym Chem 1997;35:2239–51.
[15] Hamley IW. In: Hamley IW, editor. Developments in block copolymer science and technology. Chichester: John Wiley and Sons Ltd.; 2004. p. 1.
[16] Krishnan PSG, Veeramani S, Vora RH, Chung TS, Uchimura SI, Sugitani H. J Chromatogr A 2002;977:207–12.
[17] Malawer EG. In: Wu CS, editor. Handbook of size exclusion chromatography. New York: Marcel Dekker Inc.; 1995. p. 8.
[18] Barton AFM. Handbook of solubility parameter and other cohesion parameters. Boca Raton, Florida: CRC Press; 1991 [chapters 5 and 14].
[19] Krevelen DWV. Properties of polymers: their correlation with chemical structural; their numerical estimation and prediction from additive group contributions. 3rd ed. Amsterdam: Elsevier; 1990 [chapters 4 and 7].
[20] Gallagher KP, Zhang X, Runt JP, Huynhba G, Lin JS. Macromolecules 1993;26:588–96.
[21] Chang SL, Yu TL, Huang CC, Chen WC, Linliu K, Lin TL. Polymer 1998;15:3479–89.
[22] Fox TG. Bull Am Phys Soc 1956;1:123.
[23] Chen TK, Chui JY, Shieh TS. Macromolecules 1997;30:5068–74.
[24] Olabisi O, Robeson LM, Shaw MT. Polymer–polymer miscibility. New York: Academic Press; 1979 [chapter 2].
[25] Haralampus N, Argiriadi P, Gilchriest A, Ashmore E, Scordalakes C, Martin W, et al. J Non-Cryst Solids 1998;235–237:428–34.
[26] Forrest JA, Veress KD, Dutcher JR. Phys Rev E 1997;56:5705–16.
[27] Arrighi V, Higgins JS, Burgess AN, Floudas G. Polymer 1998;25: 6369–76.
[28] Yang H, Nguyen QT, Ding YD, Long YC, Ping Z. J Membr Sci 2000; 164:37–43.